Inorg. Chem. **2003**, *42*, 7086–7097

Electroswitchable Photoluminescence Activity: Synthesis, Spectroscopy, Electrochemistry, Photophysics, and X-ray Crystal and Electronic Structures of $[Re(bpy)(CO)_3(C{\equiv}C{-}C_6H_4{-}C{\equiv}C)Fe(C_5Me_5)(dppe)][PF_6]_n$ (n = 0, 1)

Keith Man-Chung Wong,[†] Sally Chan-Fung Lam,[†] Chi-Chiu Ko,[†] Nianyong Zhu,[†] Vivian Wing-Wah Yam,*[,†] Séverine Roué,[‡] Claude Lapinte,*[,‡] Sofiane Fathallah,[§] Karine Costuas,[§] Samia Kahlal,[§] and Jean-François Halet*[,§]

Centre for Carbon-Rich Molecular and Nano-Scale Metal-Based Materials Research and Department of Chemistry, The University of Hong Kong, Pokfulam Road, Hong Kong, Organométalliques et Catalyse: Chimie et Electrochimie Moléculaire, UMR 6509 CNRS—Université de Rennes 1, Institut de Chimie de Rennes, Campus de Beaulieu, F-35042 Rennes, France, and Laboratoire de Chimie du Solide et Inorganique Moléculaire, UMR 6511 CNRS—Université de Rennes 1, Institut de Chimie de Rennes, Campus de Beaulieu, F-35042 Rennes, France

Received July 15, 2003

A novel heterobimetallic alkynyl-bridged complex, $[Re(bpy)(CO)_3(C{\equiv}C{-}C_6H_4{-}C{\equiv}C)Fe(C_5Me_5)(dppe)]$, **1**, and its oxidized species, $[Re(bpy)(CO)_3(C{\equiv}C{-}C_6H_4{-}C{\equiv}C)Fe(C_5Me_5)(dppe)][PF_6]$, **2**, have been synthesized and their X-ray crystal structures determined. A related vinylidene complex, $[Re(bpy)(CO)_3(C{\equiv}C{-}C_6H_4{-}(H)C{=}C)Fe(C_5Me_5)(dppe)][PF_6]$, **3**, has also been synthesized and characterized. The cyclic voltammogram of **1** shows a quasireversible reduction couple at –1.49 V (vs SCE), a fully reversible oxidation at –0.19 V, and a quasireversible oxidation at +0.88 V. In accord with the electrochemical results, density-functional theory calculations on the hydrogen-substituted model complex $Re(bpy)(CO)_3(C{\equiv}C{-}C_6H_4{-}C{\equiv}C)Fe(C_5H_5)(dHpe)$ ($Cp = C_5H_5$, $dHpe = H_2P{-}(CH_2)_2{-}PH_2$) (**1-H**) show that the LUMO is mainly bipyridine ligand π^* in character while the HOMO is largely iron(II) d orbital in character. The electronic absorption spectrum of **1** shows low-energy absorption at 390 nm with a 420 nm shoulder in CH_2Cl_2, while that of **2** exhibits less intense low-energy bands at 432 and 474 nm and additional low-energy bands in the NIR at ca. 830, 1389, and 1773 nm. Unlike the related luminescent rhenium(I)–alkynyl complex $[Re(bpy)(CO)_3(C{\equiv}C{-}C_6H_4{-}C{\equiv}C{-}H)]$, **4**, complex **1** is found to be nonemissive, and such a phenomenon is attributed to an intramolecular quenching of the emissive $d\pi(Re) \rightarrow \pi^*(bpy)$ ^{3}MLCT state by the low-lying MLCT and LF excited states of the iron moiety. Interestingly, switching on of the luminescence property derived from the $d\pi(Re) \rightarrow \pi^*(bpy)$ ^{3}MLCT state can be demonstrated in the oxidized species **2** and the related vinylidene analogue **3** due to the absence of the quenching pathway.

Introduction

The luminescence properties of d^6 transition metal polypyridyl complexes have been extensively studied, and there has been an increasing interest in the use of these systems in the development of new metal-based luminescent materials and sensing probes.[1] The rhenium(I) tricarbonyl diimine system, $[Re(diimine)(CO)_3X]^{0/+}$ (X = pyridyl or halide), is one of the representative systems that exhibits strong

* To whom correspondence should be addressed. E-mail: wwyam@hku.hk (V.W.-W.Y.); lapinte@univ-rennes1.fr (C.L.); halet@univ-rennes1.fr (J.-F.H.).
[†] University of Hong Kong.
[‡] Organométalliques et Catalyse: Chimie et Electrochimie Moléculaire.
[§] Laboratoire de Chimie du Solide et Inorganique Moléculaire.

(1) (a) Keefe, M. H.; Benkstein, K. D.; Hupp, J. T. *Coord. Chem. Rev.* **2000**, *205*, 201. (b) Balzani, V.; Scandola, F. *Supramolecular Photochemistry*; Ellis Horwood: Chichester, U.K., 1991. (c) Kalyanasundaram, K. *Photochemistry of Polypyridine and Porphyrin Complexes*; Academic Press: London, 1992. (d) Horváth, O.; Stevenson, K. L. *Charge-Transfer Photochemistry of Coordination Compounds*; VCH: New York, 1993.

10.1021/ic030226d CCC: $25.00
Published on Web 10/01/2003

luminescence derived from the dπ(Re) → π*(diimine) metal-to-ligand charge transfer (MLCT) triplet excited state.[2] There are a number of advantages associated with such inorganic/organometallic MLCT systems. A large energy difference between the absorption and emission energies, i.e., large Stokes' shift, would minimize the interference due to the excitation source on the detection. The luminescence intensity and energy are sensitive to changes in the environment, and the luminescence lifetime, which comes from the phosphorescence, is usually comparatively long. The emission energy can be easily tuned by the systematic variation of the diimine and the spectator ligands in view of the versatility of the synthetic methods to these systems. Despite the fact that there has been a rapidly growing interest in the chemistry of transition metal−alkynyl compounds with a conjugated π-system as a result of the unique physical properties observed in a number of such systems,[3] reports on the luminescence behavior of this type of complexes are relatively scarce.[4,5] Preparation of luminescent rhenium(I)−alkynyl complexes, [Re(diimine)(CO)$_3$(C≡C)$_n$−R], has recently been reported by Yam et al. through the incorporation of the alkynyl group into the rhenium(I) tricarbonyl diimine luminophore, and their luminescence behavior has been systematically investigated. The luminescence behavior has been found to be perturbed by a systematic variation of the diimine and the R group on the alkynyl as well as the number of C≡C units.[6]

On the other hand, various polynuclear organoiron compounds of different geometries, where electroactive [(C$_5$Me$_5$)(dppe)Fe] units are linked together, either directly through polyynyl bridges or via a central organic spacer by means of an ethynyl bridge, have been studied. In these compounds, the intimate combination of metal atoms with carbon-rich ligands gives rise to unusual properties such as efficient long-distance electron transfer, and strong magnetic exchange interaction between the remote iron termini.[3a,7] In addition, a heterobimetallic iron(II)−rhenium(I) butadiynyl complex, [(C$_5$Me$_5$)(dppe)Fe(C≡C−C≡C)Re(C$_5$Me$_5$)(NO)(PPh$_3$)], recently demonstrated a "conjugal" redox family with interesting electronic communication between the two termini groups.[8] These have prompted us to combine the strongly emissive [Re(diimine)(CO)$_3$(C≡C−R)] fragment and redox active [(C$_5$Me$_5$)(dppe)Fe(C≡C−R)] moiety by a diyndiyl ligand to form another new type of heterobimetallic iron(II)−rhenium(I) complex, [Re(diimine)(CO)$_3$(C≡C−R−C≡C)Fe(C$_5$Me$_5$)(dppe)]. It is envisaged that the luminescence properties of the rhenium(I) tricarbonyl diimine system would

Scheme 1

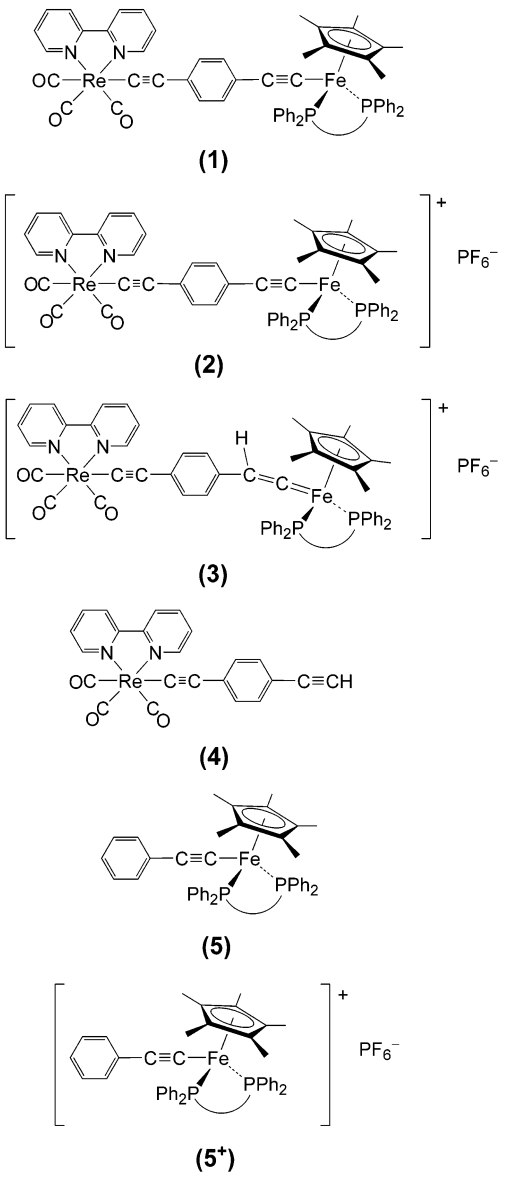

(2) (a) Wrighton, M. S.; Morse, D. L. *J. Am. Chem. Soc.* **1974**, *96*, 998. (b) Wrighton, M. S.; Morse, D. L.; Pdungsap, L. *J. Am. Chem. Soc.* **1975**, *97*, 2073.

(3) (a) Paul, F.; Lapinte, C. *Coord. Chem. Rev.* **1998**, *178*−*180*, 431. (b) Bruce, M. I. *Coord. Chem. Rev.* **1997**, *166*, 91. (c) Lang, H. *Angew. Chem., Int. Ed. Engl.* **1994**, *33*, 547. (d) Puddephatt, R. J. *Chem. Commun.* **1998**, 1055. (e) Schwab, P. F. H.; Levin, M. D.; Michl, J. *Chem. Rev.* **1999**, *99*, 1863. (f) Bunz, U. H. F. *Angew. Chem., Int. Ed. Engl.* **1996**, *35*, 969. (g) Stahl, J.; Bohling, J. C.; Bauer, E. B.; Peters, T. B.; Mohr, W.; Martín-Alvarez, J. M.; Hampel, F.; Gladysz, J. A. *Angew. Chem., Int. Ed.* **2002**, *41*, 1871.

(4) (a) Yam, V. W. W.; Lo, K. K. W.; Wong, K. M. C. *J. Organomet. Chem.* **1999**, *578*, 3. (b) Yam, V. W. W. *Acc. Chem. Res.* **2002**, *35*, 555. (c) Yam, V. W. W.; Tang, R. P. L.; Wong, K. M. C.; Cheung, K. K. *Organometallics* **2001**, *20*, 4476. (d) Yam, V. W. W.; Wong, K. M. C.; Zhu, N. *J. Am. Chem. Soc.* **2002**, *124*, 6506. (e) Yam, V. W. W.; Wong, K. M. C.; Zhu, N. *Angew. Chem., Int. Ed.* **2003**, *42*, 1400.

(5) (a) Adams, C. J.; James, S. L.; Liu, X.; Raithby, P. R.; Yellowless, L. J. *J. Chem. Soc., Dalton Trans.* **2000**, 63. (b) Whittle, C. E.; Weinstein, J. A.; George, M. W.; Schanze, K. S. *Inorg. Chem.* **2001**, *40*, 4053. (c) McGarrah, J. E.; Kem, Y. J.; Hissler, M.; Eisenberg, R. *Inorg. Chem.* **2001**, *40*, 4510. (d) Lu, W.; Mi, B. X.; Chan, M. C. W.; Hui, Z.; Zhu, N.; Lee, S. T.; Che, C. M. *Chem. Commun.* **2002**, 206. (e) Chan, S. C.; Chan, M. C. W.; Wang, Y.; Che, C. M.; Cheung, K. K.; Zhu, N. *Chem. Eur. J.* **2001**, *7*, 4180. (f) Ara, I.; Forniés, J.; Gómez, J.; Lalinde, E.; Moreno, M. T. *Organometallics* **2000**, *19*, 3137. (g) Berenguer, J. R.; Forniés, J.; Gómez, J.; Lalinde, E.; Moreno, M. T. *Organometallics* **2001**, *20*, 4847.

(6) (a) Yam, V. W. W. *Chem. Commun.* **2001**, 789. (b) Yam, V. W. W.; Lau, V. C. Y.; Cheung, K. K. *Organometallics* **1995**, *14*, 2749. (c) Yam, V. W. W.; Lau, V. C. Y.; Cheung, K. K. *Organometallics* **1996**, *15*, 1740. (d) Yam, V. W. W.; Chong, S. H. F.; Cheung, K. K. *Chem. Commun.* **1998**, 2121. (e) Yam, V. W. W.; Chong, S. H. F.; Ko, C. C.; Cheung, K. K. *Organometallics* **2000**, *19*, 5092.

(7) Paul, F.; Lapinte, C. In *Physical Organometallic Chemistry*; Gielen, M., Willem, R., Wrackmeyer, B., Eds.; John Wiley: London, 2002; p 220−291.

(8) Paul, F.; Meyer, W. E.; Toupet, L.; Jiao, H.; Gladysz, J. A.; Lapinte, C. *J. Am. Chem. Soc.* **2000**, *122*, 9405.

Scheme 2

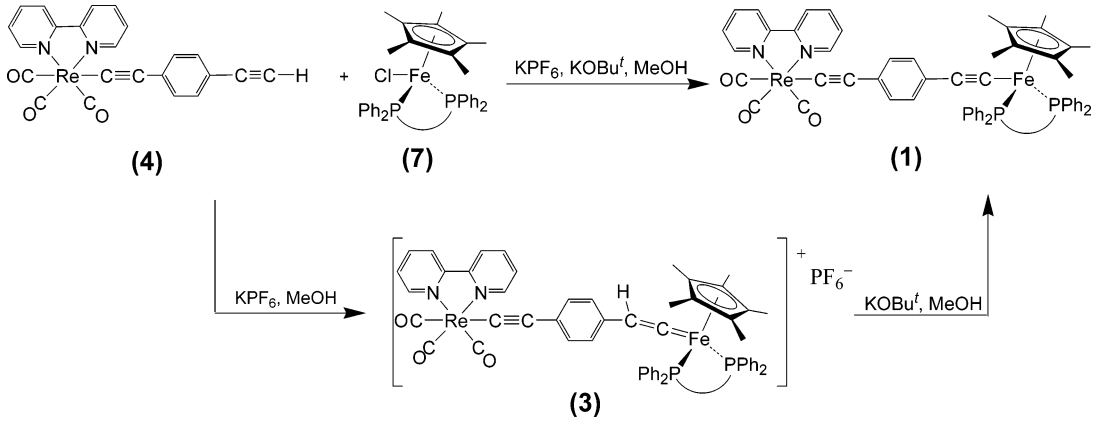

be perturbed, varied, or even switched on/off, by the coordination of the iron(II) fragment as well as the oxidation of the iron(II) center to iron(III). Herein, we report the synthesis of a novel heterobimetallic iron(II)−rhenium(I) complex, $[Re(bpy)(CO)_3(C{\equiv}C{-}C_6H_4{-}C{\equiv}C)Fe(C_5Me_5)(dppe)]$ (**1**), by the reaction of the corresponding precursor complexes $[Re(bpy)(CO)_3(C{\equiv}C{-}C_6H_4{-}C{\equiv}C{-}H)]$ (**4**) and $[Fe(C_5Me_5)(dppe)Cl]$ (**7**). Its corresponding one-electron oxidized species, $[Re(bpy)(CO)_3(C{\equiv}C{-}C_6H_4{-}C{\equiv}C\text{-})Fe(C_5Me_5)(dppe)](PF_6)$ (**2**), and the related vinylidene complex, $[Re(bpy)(CO)_3(C{\equiv}C{-}C_6H_4{-}CH{=}C{=})Fe(C_5Me_5)(dppe)](PF_6)$ (**3**), have also been synthesized (Scheme 1). A systematic comparison of the electrochemical behavior, electronic absorption spectroscopy, and luminescence properties of these complexes with the related mononuclear complexes, $[(C_5Me_5)(dppe)Fe(C{\equiv}C{-}C_6H_5)]$ (**5**) and $[(C_5Me_5)(dppe)Fe(C{\equiv}C{-}C_6H_5)](PF_6)$ (**5**$^+$), has been made. The X-ray crystal structures of **1** and **2** have been determined, and their electronic structures have also been computed.

Results and Discussion

Synthesis and Characterization of 1. Complex **1** was prepared from the iron chloride $(C_5Me_5)(dppe)FeCl$ (**7**)[9] and the rhenium complex $[Re(bpy)(CO)_3(C{\equiv}C{-}C_6H_4{-}C{\equiv}CH)]$ (**4**).[10] Treatment of 1 equiv of **4** with 1.1 equiv of **7** in a $CH_3OH-THF$ mixture (3:1 v/v) and in the presence of KPF_6 and KO^{t}Bu produced, after stirring for 48 h at 20 °C, an orange-brown solution. The heterobinuclear complex **1** was isolated from this solution as a brownish yellow powder in 40% yield after recrystallization from a $CH_2Cl_2-CH_3OH$ mixture. The PF_6^- anion was used to promote the complexation of the terminal alkyne at the iron center, which affords the vinylidene intermediate in situ, which is deprotonated by the base (Scheme 2). The reaction was also carried out in the absence of base to yield the binuclear iron vinylidene−rhenium alkynyl complex **3**, isolated as a brown powder (yield 75%). Compounds **1** and **3** gave correct elemental analyses and were characterized by multinuclear NMR spectroscopy. FAB mass spectra of **1** and **3** showed the expected parent ions.

Table 1. IR Data for **1**, **2**, **3**, and the Related Mononuclear Compounds **4** and **5**

complex	medium	$\nu_{C\equiv C}$ (cm^{-1})	$\nu_{C\equiv O}$ (cm^{-1})	ref
1	KBr/Nujol	2055 (w), 2038 (w)	2005 (s), 1909 (s), 1898 (s)	this work
	CH_2Cl_2	2052 (w), 2033 (w)	2007 (s, br), 1903 (s)	
2	KBr/Nujol	2085 (w), 1980 (w)	2003 (s, br), 1888 (s)	this work
	CH_2Cl_2	2085 (w), 1980 (w)	2007 (s, br), 1888 (s)	
3	KBr/Nujol	2087 (w), 2061 (sh), 1617 (w)	2001 (s, br), 1880 (s)	this work
	CH_2Cl_2	2083 (w), 1625 (w)	2007 (s, br), 1904 (s)	
4	KBr/Nujol	2081 (w)	2004 (s), 1916 (s), 1888 (s)	10
5	KBr/Nujol	2049 (w)		12
	CH_2Cl_2	2053 (w)		
5$^+$	KBr/Nujol	2025 (w), 1993 (sh)		12
	CH_2Cl_2	2021 (w), 1988 (w)		

In the FTIR spectrum of compound **1**, the rhenium tricarbonyl center was evidenced by the presence of three intense carbonyl stretching modes expected for a $M(CO)_3$ fragment in a facial arrangement.[11] The most intense band is split in the spectra run with a Nujol mull sample due to solid state effects. Complex **1** is also characterized by two weak infrared absorptions at 2052 and 2033 (cm^{-1}, CH_2Cl_2), which correspond to the C≡C stretching modes. For the Re^I and Fe^{II} monometallic parent compounds **4** and **5**, a single C≡C stretching band due to the C≡C bond adjacent to Re^I or Fe^{II} is observed at 2081 and 2053 cm^{-1}, respectively (Table 1). The shift toward the lower frequency of the C≡C bond stretching (ca. 20−30 cm^{-1}) in the bimetallic complex relative to the related mononuclear derivatives reflects the interaction of the iron and rhenium center through the carbon-rich bridging ligand. This shift suggests a slight decrease in the triple bond order in the bimetallic compounds. For Fe^{II} complexes of the series $[(C_5Me_5)(dppe)Fe(C{\equiv}C\text{-}1,4\text{-}C_6H_4{-}X)]$, it has been shown that a diminution in the alkynyl bond order takes place when X is a strongly electron-withdrawing substituent.[12,13] The iron and rhenium metal centers act as donor and acceptor, respectively, and complex **1** is polarized, accordingly. Analyzed from a valence bond (VB) standpoint, the weight of the VB structure B (Scheme 3) cannot be neglected in the bonding description.

(9) Roger, C.; Hamon, P.; Toupet, L.; Rabaâ, H.; Saillard, J. Y.; Hamon, J. R.; Lapinte, C. *Organometallics* **1991**, *10*, 1045.
(10) Wong, K. M. C. Ph.D. Thesis, The University of Hong Kong, 1998.
(11) Stufkens, D. J. *Coord. Chem. Rev.* **1990**, *104*, 39.
(12) Denis, R.; Toupet, L.; Paul, F.; Lapinte, C. *Organometallics* **2000**, *19*, 4240.
(13) Paul, F.; Mevellec, J. Y.; Lapinte, C. *J. Chem. Soc., Dalton Trans.* **2002**, 1783.

Scheme 3

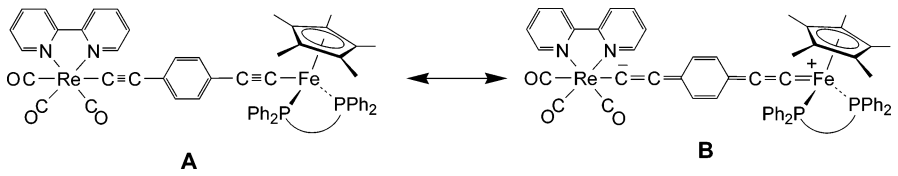

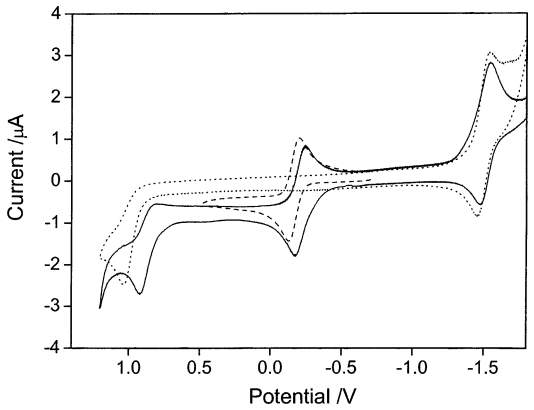

Figure 1. Cyclic voltammograms of **1** (—) and related monometallic complexes **4** (- - -) and **5** (— — —) in 0.1 M $^{n}Bu_4NPF_6/CH_2Cl_2$ (Pt electrode, V vs SCE, scan rate 0.100 V/s, 20 °C).

The presence of a deshielded C_α triplet (δ_C 363, $^2J_{CP}$ = 34 Hz) typical of metalla-vinylidene in the ^{13}C NMR spectrum of **3** supports the proposed structure.[14] In addition, the FTIR spectrum of compound **3** displays a band at 1625 (cm^{-1}, CH_2Cl_2), characteristic of the metal vinylidene derivatives, while the Re—C≡C stretching mode is located at a slightly higher frequency relative to the mononuclear complex **4** ($\Delta\nu$ = 6 cm^{-1}), indicating that the cationic iron vinylidene site introduces a perturbation similar to the oxidation of the iron site on the rhenium endgroup (see following description).

As illustrated in Figure 1, the cyclic voltammogram of **1** shows the quasireversible reduction couple of the rhenium site at −1.49 V, and the fully reversible oxidation of the iron site at −0.19 V. A third almost reversible oxidation wave corresponding to the formation of a dicationic species is observed at the solvent edge. Cyclic voltammograms of the related monometallic rhenium complex **4** and iron complex **5** were measured under identical conditions. The cyclic voltammogram of iron complex **5** presents a reversible oxidation wave at E_0 = −0.15 V, corresponding to the redox system Fe^{II}/Fe^{III}. At a much more positive potential (E_0 = +1.34 V, not shown in Figure 1), an irreversible oxidation process is also observed. The cyclic voltammogram of the mononuclear rhenium complex **4** displays a reversible reduction wave and an irreversible oxidation wave at +1.05 V. Analysis of the E_0 values (Table 2) reveals weak electronic interactions between the metal endgroups. Specifically, substitution of the terminal alkyne in **4** by the [(C_5Me_5)-(dppe)Fe] moiety renders the reduction of the rhenium endgroup 0.02 V less favorable, while the introduction of the [Re(bpy)(CO)$_3$(C≡C)—] fragment at the *para* position of the aryl ring in complex **5** renders the oxidation of the iron site 0.04 V more favorable. These data show that both the iron and rhenium endgroups act as electron-releasing groups toward the opposite termini which facilitate the oxidation and make the reduction slightly more difficult. In other words, the electron-rich Fe^{II} site stabilizes the Re^{I} termini, while the electron-demanding Fe^{III} end is stabilized by the Re^{I} site. Finally, the CV data show that the one-electron oxidation product of **1** constitutes a synthetic accessible target, and it can be anticipated that the electron vacancy will be mainly located on the iron center. On the other hand, the second oxidation observed at +0.88 V which should be rhenium-centered occurs in the binuclear complex at a potential 0.17 V more favorable than in the parent rhenium derivative. It seems that the Fe^{III} center should be able to act as an electron-releasing group for the Re^{II} center in the dication.

Table 2. Electrochemical Data for **1**, **4**, and **5**

complex	$E°$ (V)	ΔE_p (V)	i_a/i_c	ref
1	−1.49	0.07	1.4	this work
	−0.19	0.07	1.0	
	+0.88	0.07	0.6	
4	−1.47	0.08	1.0	this work
	+1.05			
	+1.78			
5	−0.15	0.08	1.0	12
	+1.34			

Synthesis and Characterization of 2. To avoid side reactions with adventitious solvent impurities, the oxidation of **1** was carried out in THF at −80 °C using 0.95 equiv of ferrocenium salt as oxidizing reagent. Due to the poor solubility of the compounds at low temperature, the reaction took 6 h to reach completion. During this time, the solution progressively turned from brown-red to deep green. Addition of a large excess of cold hexane precipitated complex **2** as a green powder, isolated in 82% yield. As expected, **1** and **2** gave identical cyclic voltammetric data.

Comparison of the FTIR spectra of **1** and **2** shows a shift of the stretching mode attributed to Fe—C≡C toward the lower energies (Δ = −58 cm^{-1}) as usually observed upon one-electron oxidation in the (C_5Me_5)(dppe)Fe series. At the same time, the Re—C≡C vibration band moves in the opposite direction (Δ = +30 cm^{-1}). The consequence of the one-electron oxidation of complex **1** on the bonding of the carbon-rich bridging ligand is weak, but it suggests that the direction of the polarization of the π-electron system of the spacer could be reversed upon electron transfer. In compound **2**, the iron and rhenium endgroups play the role of the acceptor and donor groups for the bridging ligand, respectively. In addition, with respect to the spectrum of **1**, the FTIR spectrum of compound **2** shows a small negative shift of the CO bond stretches ($-1 < \Delta\nu < -10$ cm^{-1}) suggesting that the oxidation of the iron center is slightly

(14) Bruce, M. I.; Swincer, A. G. *Adv. Organomet. Chem.* **1983**, *22*, 59.

sensed by the rhenium site and does not contribute to reduce the electronic density at rhenium in agreement with the CV data (see preceding discussion).

Complex **2** was characterized by ^{57}Fe Mössbauer spectroscopy at 80 K. The spectrum recorded at zero field gives a doublet typical of an Fe^{III} metal center in the [(C_5Me_5)(dppe)Fe] series ($\delta = 0.259$ mm/s vs Fe, $\Gamma = 0.214$ mm/s, QS = 0.898 mm/s). These values are very close to the data previously reported for complex $\mathbf{5}^+$ ($\delta = 0.255$ mm/s vs Fe, QS = 0.900 mm/s), which clearly shows that the electronic perturbation introduced by the rhenium endgroup is only very weakly sensed by the iron center. Mössbauer spectroscopy unambiguously establishes that the oxidation takes place at the iron center and complex **2** is best represented by Fe^{III} and Re^{I} metal centers spanned by the 1,4-diethynylbenzene ligand.

The fluid-solution ESR spectrum of the radical cation **2** shows a broad singlet. However, in a low-temperature glass the ESR spectrum of **2** (77 K, CH_2Cl_2/$ClCH_2CHCl$, 1:1 v/v) displays three well separated features corresponding to the three components of the *g*-tensor appropriate for a pseudo-octahedral geometry around the radical.[3a] No hyperfine coupling with P or Re nuclei could be observed. The tensor values ($g_1 = 1.981$, $g_2 = 2.035$, $g_3 = 2.422$) are again typical of a low-spin 17-electron iron-centered radical. A very similar spectrum was previously obtained for the parent radical $\mathbf{5}^+$ ($g_1 = 1.975$, $g_2 = 2.033$, $g_3 = 2.464$). The slightly smaller g_3 value in **2** than $\mathbf{5}^+$ suggests weaker interactions between the single electron and electrons of lower-lying orbitals.[15] The smaller SOMO/(SOMO − 1) energy separation in **2** relative to $\mathbf{5}^+$ can be attributed to the effect of the [Re(CO)$_3$(bpy)(C≡C)−] endgroup. Moreover, the reduced anisotropy of the *g*-tensor ($\Delta g = g_3 - g_1 = 0.441$) relative to the monometallic radical $\mathbf{5}^+$ ($\Delta \boldsymbol{g} = 0.489$) would indicate an increased delocalization of the SOMO in the bimetallic radical.

Crystal Structures of 1 and 2. Perspective drawings of **1** and **2** are depicted in Figures 2a and b, respectively. Their crystal structure determination data are summarized in Table 3, and selected bond distances and angles are given in Table 4.

Complexes **1** and **2** show a similar structure, comprising rhenium(I) and iron(II) or iron(III) connected by a 1,4-diethynylbenzene bridge. In both cases, the coordination about the rhenium(I) metal center adopts a distorted octahedral geometry with the three carbonyl ligands arranged in a facial fashion while the iron(II) or iron(III) fragment, coordinated with one C_5Me_5, one dppe, and one alkynyl group, exhibits a pseudo-octahedral geometry as commonly found in other piano-stool complexes. Similar coordination geometries have been found in the related rhenium(I)−alkynyl complexes, [Re(N−N)(CO)$_3$(C≡C−R)] (N−N = diimine ligand, R = aromatic groups)[6] and iron(II)− or iron(III)−alkynyl complexes, [(C_5Me_5)(dppe)Fe(C≡C−R)]$^{0/+}$.[12] The bond distances and bond angles of the [Re(bpy)(CO)$_3$(C≡C−)] and [(C_5Me_5)(dppe)Fe(C≡C−)]$^{0/+}$ units are comparable to their mononuclear counterparts.[6,12] The bond angles of N(1)−Re(1)−N(2) [**1**, 74.3(2) °; **2**, 74.45(19) °] are found to be less than 90° as required by the bite distance exerted by the steric demand of the chelating bipyridine ligand. On the other hand, smaller deviations from the ideal 90° are observed for the P(1)−Fe(1)−P(2) angles [**1**, 86.31(6)°; **2**, 83.20(5)°] on the [(C_5Me_5)(dppe)Fe(C≡C−)]$^{0/+}$ moieties due to the larger bite angle and the more flexible nature of the dppe ligand. The bond angles of Re(1)−C(1)−C(2) [**1**, 171.8(6)°; **2**, 173.9(4)°] and C(1)−C(2)−C(3) [**1**, 174.4(7)°; **2**, 175.4(5)°] in the [Re(bpy)(CO)$_3$(C≡C−)] unit as well as those of C(6)−C(9)−C(10) [**1**, 178.6(6)°; **2**, 176.6(5)°] and C(9)−C(10)−Fe(1) [**1**, 178.6(6)°; **2**, 176.3(5)°] in the [(C_5Me_5)(dppe)Fe(C≡C−)]$^{0/+}$ units indicate only slightly distorted linear arrangements, as anticipated for the sp hybridization of the C≡C bond in the alkynyl moiety. The slight deviation from perfect linearity of the bond angles may be ascribed to intramolecular steric interaction between the [Re(bpy)(CO)$_3$(C≡C−)] and the [(C_5Me_5)(dppe)Fe(C≡C−)]$^{0/+}$ fragments, similar to the phenomenon commonly observed in other binuclear alkynyl-containing transition metal complexes.[3g,5c,7,12] The bond distances of C(1)−C(2) [**1**, 1.186(9) Å; **2**, 1.207(7) Å] and C(9)−C(10) [**1**, 1.223(9) Å; **2**, 1.219(7) Å] are typical of C≡C bond distances found in other metal−alkynyl systems,[3−8,12−14,16] while those of Re(1)−C(1) [**1**, 2.159(6) Å; **2**, 2.127(5) Å] and Fe(1)−C(10) [**1**, 1.891(6) Å; **2**, 1.890(6) Å] are comparable to their

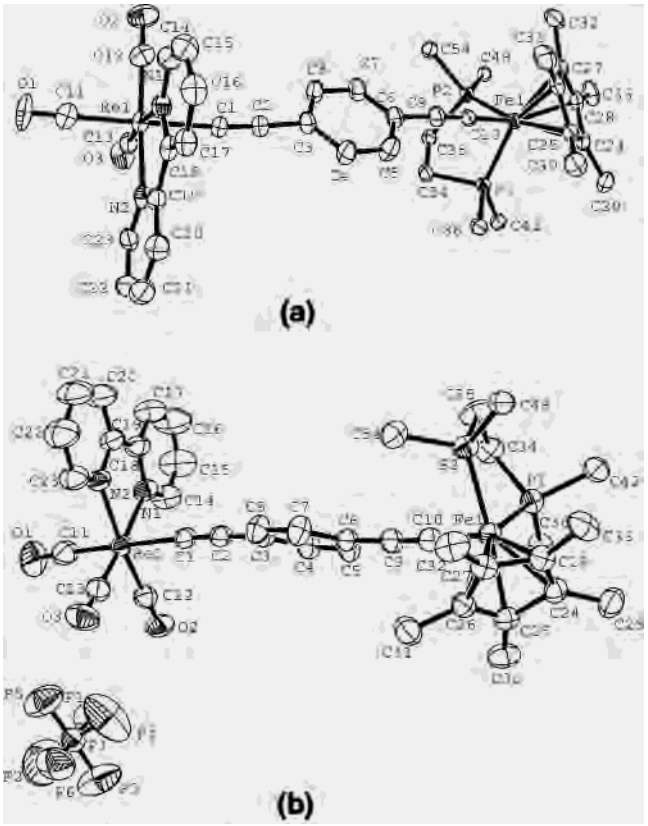

Figure 2. Perspective drawings of **1** (a) and **2** (b) with atomic numbering. Thermal ellipsoids are at the 30% probability level. Hydrogen atoms and dichloromethane molecules are omitted, and only the *ipso* carbons of the phenyl rings attached to dppe are shown for clarity.

(15) Weyland, T.; Costuas, K.; Mari, A.; Halet, J. F.; Lapinte, C. *Organometallics* **1998**, *17*, 5569.

Table 3. Crystal Data and Structure Refinement Parameters for **1** and **2**

	1·2CH_2Cl_2	**2**·1.5CH_2Cl_2
empirical formula	[$C_{61}H_{55}Cl_4FeN_2O_3P_2Re$]	[$C_{60.5}H_{54}Cl_3F_6FeN_2O_3P_3Re$]
fw	1309.86	1412.37
T (K)	301	301
cryst dimens (mm^3)	0.4 × 0.25 × 0.1	0.5 × 0.3 × 0.2
cryst syst	triclinic	monoclinic
space group	$P\bar{1}$	$P2_1/n$
unit cell demensions		
a (Å)	11.956(2)	13.160(3)
b (Å)	15.308(2)	15.100(3)
c (Å)	17.385(3)	33.363(7)
α (deg)	68.47(2)	90
β (deg)	86.33(2)	94.10(3)
γ (deg)	75.59(2)	90
Z	2	4
V ($Å^3$)	2865.5(8)	6613(2)
D_{calcd} (g cm^{-3})	1.518	1.419
F(000)	1316	2824
λ (graphite monochromated Mo Kα) (Å)	0.71073	0.71073
μ (mm^{-1})	2.652	2.300
collection range	$2\theta_{max} = 51.16^o$	$2\theta_{max} = 51.20^o$
index ranges	$-13 \le h \le 13$	$-15 \le h \le 14$
	$-18 \le k \le 18$	$-17 \le k \le 18$
	$-20 \le l \le 21$	$-40 \le l \le 40$
no. reflns collected	21402	29932
no. unique reflns	9907 [$R_{int} = 0.0411$]	10063 [$R_{int} = 0.0544$]
completeness to $\Delta = 25.58°$	91.9%	80.8%
data/restraints/params	9907/3/649	10063/0/757
final R indices[a] [$I > 2\sigma(I)$]	$R1 = 0.0495$	$R1 = 0.0406$
	$wR2 = 0.1430$	$wR2 = 0.0935$
R indices (all data)	$R1 = 0.0590$	$R1 = 0.0698$
	$wR2 = 0.1543$	$wR2 = 0.1012$
GOF, S	1.071	0.907
max peak, hole (e $Å^{-3}$)	1.583, −1.328	0.670, −0.368

[a] $w = 1/[\sigma^2(F_o^2) + (aP)^2 + bP]$; $P = [2F_c^2 + \max(F_o^2, 0)]/3$.

corresponding mononuclear counterparts, [Re(N−N)$(CO)_3$(C≡C−R)][6] and [(C_5Me_5)(dppe)Fe(C≡C−R)]$^{0/+}$.[12,16] The separation between Re(1) and Fe(1) are 12.06 and 12.08 Å in **1** and **2**, respectively, demonstrating that there is very little contraction or expansion of the molecules. Although the crystal structures of **1** and the complex cation of **2** are similar, it is noteworthy that some of the features are different. A scrutiny of their bond distances shows that the Fe−P bonds are shorter in the neutral compound **1** (2.1888−2.1985 Å) relative to that in the corresponding one-electron oxidized species **2** (2.2558−2.2633 Å). This could be attributed to the presence of the strong metal-to-ligand π-back-bonding from the electron-rich iron(II) metal center in **1** compared to that of the electron-deficient iron(III) center in **2**. As previously noted in the case of the mononuclear iron complexes,[12] the bond distances of Fe(1)−C(10) [**1**, 1.891(6) Å; **2**, 1.890(6) Å] and C(9)−C(10) [**1**, 1.223(9) Å; **2**, 1.219(7) Å] are relatively insensitive to the oxidation state of the iron center. It is interesting to note that a slight shortening of the Re(1)−C(1) bonds [**1**, 2.159(6) Å; **2**, 2.127(5) Å] with a concomitant tendency toward elongation of the C(1)−C(2) bonds [**1**, 1.186(9) Å; **2**, 1.207(7) Å] is observed in the rhenium(I)−alkynyl unit upon oxidation of **1** to **2**. This may be rationalized that the [Re(bpy)$(CO)_3$(C≡C−)] unit in **2** would show a stronger rhenium-to-alkynyl

(16) Weyland, T.; Ledoux, I.; Brasselet, S.; Zyss, J.; Lapinte, C. *Organometallics* **2000**, *19*, 5235.

Table 4. Selected Bond Distances (Å) and Bond Angles (deg) for **1** and **2**

	1	**2**
Bond Distances (Å)		
Re(1)−C(1)	2.159(6)	2.127(5)
Re(1)−N(1)	2.175(5)	2.187(4)
Re(1)−N(2)	2.205(6)	2.187(4)
Re(1)−C(11)	1.983(8)	1.946(8)
Re(1)−C(12)	1.923(9)	1.940(8)
Re(1)−C(13)	1.921(8)	1.901(8)
C(11)−O(1)	1.106(10)	1.151(9)
C(12)−O(2)	1.158(10)	1.137(8)
C(13)−O(3)	1.150(9)	1.169(8)
C(1)−C(2)	1.186(9)	1.207(7)
C(2)−C(3)	1.448(9)	1.448(8)
C(6)−C(9)	1.440(8)	1.438(8)
C(9)−C(10)	1.223(9)	1.219(7)
Fe(1)−C(10)	1.891(6)	1.890(6)
Fe(1)−P(1)	2.1888(17)	2.2558(13)
Fe(1)−P(2)	2.1985(16)	2.2633(15)
Bond Angles (deg)		
C(11)−Re(1)−C(1)	178.6(3)	179.5(3)
C(12)−Re(1)−N(2)	172.7(3)	173.4(2)
C(13)−Re(1)−N(1)	171.7(2)	171.9(2)
Re(1)−C(1)−C(2)	171.8(6)	173.9(4)
Re(1)−C(11)−O(1)	175.4(8)	177.0(7)
Re(1)−C(12)−O(2)	179.1(7)	178.2(5)
Re(1)−C(13)−O(3)	179.2(7)	179.0(6)
N(1)−Re(1)−N(2)	74.3(2)	74.45(19)
C(1)−C(2)−C(3)	174.4(7)	175.4(5)
C(6)−C(9)−C(10)	172.9(7)	176.6(5)
C(9)−C(10)−Fe(1)	178.6(6)	176.3(5)
P(1)−Fe(1)−P(2)	86.31(6)	83.20(5)
P(1)−Fe(1)−C(10)	81.64(18)	86.61(14)
P(2)−Fe(1)−C(10)	87.94(18)	86.87(16)

π-back-donation to the π^*(C≡C−R−C≡C) orbital of the electron-deficient iron(III)-substituted diethynylbenzene unit, leading to a shortening of the Re(1)−C(1) bond and an elongation of the C(1)−C(2) bond. This is indicative of the presence of weak electronic communication across the alkynyl bridge between the two endgroups.

Electronic Structures. In order to study the electronic structure of **1**, quantum chemical calculations were carried out at the B3LYP level of density functional theory using the Gaussian-98 suite of programs[17] on the hydrogen-substituted model complex, Re(bpy)$(CO)_3$(C≡C−C_6H_4−C≡C)Fe(Cp)(dHpe) (Cp = C_5H_5, dHpe = $H_2P-(CH_2)_2-PH_2$) (**1-H**) of C_s symmetry. In order to compare and contrast their electronic structures to that of **1-H**, calculations were performed as well on the parent molecules Re(bpy)$(CO)_3$(C≡C−C_6H_4−C≡CH) (**4**) and Fe(Cp)(dHpe)(C≡C−C_6H_4−C≡CH) (**6-H**) containing the same spacer. The latter is related to Fe(C_5Me_5)(dppe)(C≡C−C_6H_4−C≡CH) (**6**) recently described.[18] Calculations were also performed on Fe-

(17) Frisch, M. J.; Trucks, G. W.; Schlegel, H. B.; Scuseria, G. E.; Robb, M. A.; Cheeseman, J. R.; Zakrzewski, V. G.; Montgomery, J. A., Jr.; Stratmann, R. E.; Burant, J. C.; Dapprich, S.; Millam, J. M.; Daniels, A. D.; Kudin, K. N.; Strain, M. C.; Farkas, O.; Tomasi, J.; Barone, V.; Cossi, M.; Cammi, R.; Mennucci, B.; Pomelli, C.; Adamo, C.; Clifford, S.; Ochterski, J.; Petersson, G. A.; Ayala, P. Y.; Cui, Q.; Morokuma, K.; Malick, D. K.; Rabuck, A. D.; Raghavachari, K.; Foresman, J. B.; Cioslowski, J.; Ortiz, J. V.; Stefanov, B. B.; Liu, G.; Liashenko, A.; Piskorz, P.; Komaromi, I.; Gomperts, R.; Martin, R. L.; Fox, D. J.; Keith, T.; Al-Laham, M. A.; Peng, C. Y.; Nanayakkara, A.; Gonzalez, C.; Challacombe, M.; Gill, P. M. W.; Johnson, B. G.; Chen, W.; Wong, M. W.; Andres, J. L.; Head-Gordon, M.; Replogle, E. S.; Pople, J. A. *Gaussian 98*, revision A.5; Gaussian, Inc.: Pittsburgh, PA, 1998.

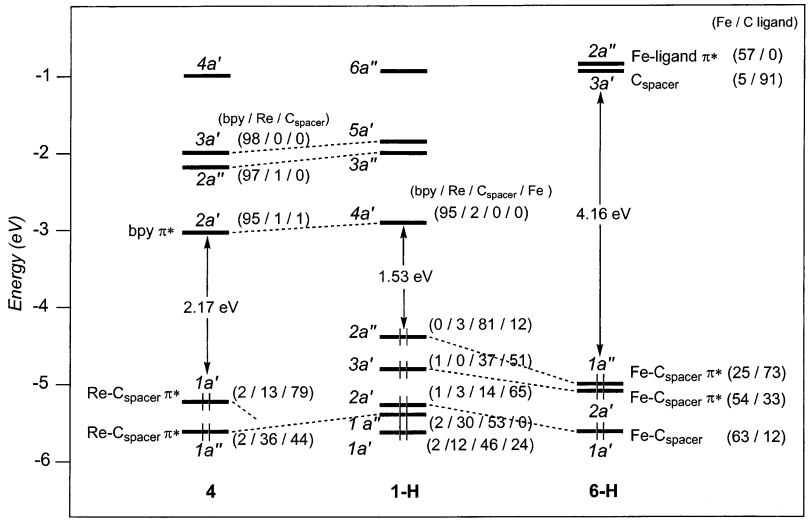

Figure 3. DFT molecular orbital diagrams of the complex models Re(bpy)(CO)$_3$(C≡C−C$_6$H$_4$−C≡C)Fe(Cp)(dHpe) (**1-H**), Re(bpy)(CO)$_3$(C≡C−C$_6$H$_4$−C≡CH) (**4**), and Fe(Cp)(dHpe)(C≡C−C$_6$H$_4$−C≡CH) (**6-H**). The ligand/metal/carbon spacer percentage contributions of the MOs are given in brackets.

Table 5. Computational Data for the Complex Models Re(bpy)(CO)$_3$(C≡C−C$_6$H$_4$−C≡C)Fe(Cp)(dHpe) (**1-H**), Re(bpy)(CO)$_3$(C≡C−C$_6$H$_4$−C≡CH) (**4**), Fe(Cp)(dHpe)(C≡C−C$_6$H$_5$) (**5-H**), and Fe(Cp)(dHpe)(C≡C−C$_6$H$_4$−C≡CH) (**6-H**)

	[**1-H**]^q			[**4**]^q		[**5-H**]^q		[**6-H**]^q	
q:	+	0	−	0	−	+	0	+	0
				Energies (eV)					
$\Delta E_{HOMO/LUMO}$	1.35	1.53	1.20	2.18	1.56	1.93	4.23	1.93	4.16
IP		5.19					5.58		5.92
EA		1.67		1.85					
				Distances (Å)					
Re−C(α)	2.09	2.11	2.12	2.11	2.11				
Re−N	2.18	2.18	2.18	2.19	2.18				
C(α)−C(β)	1.25	1.24	1.24	1.23	1.24			1.22	1.23
Fe−C(α′)	1.84	1.92	1.92			1.86	1.92	1.89	1.91
C(α′)−C(β′)	1.26	1.24	1.25	1.22	1.23	1.25	1.25	1.24	1.25
Fe−C(Cp)	2.19	2.19	2.19			2.20	2.19	2.20	2.19
Fe−P	2.31	2.29	2.28			2.34	2.26	2.33	2.27
				Mulliken Charges					
Re	+0.69	+0.68	+0.70	+0.65	+0.69				
C(α)	−0.05	−0.10	−0.06	−0.09	−0.05				
C(β)	−0.37	−0.37	−0.39	−0.34	−0.36				
Fe	−0.63	−0.61	−0.56			−0.60	−0.58	−0.56	−0.59
C(α′)	+0.10	+0.05	+0.02			+0.03	+0.06	+0.00	+0.08
C(β′)	−0.21	−0.27	−0.26			−0.13	−0.25	−0.12	−0.26
				Spin Densities					
bpy	+0.00		+0.90		+0.98				
Re	+0.02		−0.01		−0.01				
C(α)	+0.13		+0.00		+0.01	+0.03			
C(β)	+0.00		+0.00		+0.00	−0.02			
Fe	+0.58		+0.00			+1.13		+1.13	
C(α′)	+0.01		+0.01			−0.02		−0.06	
C(β′)	+0.16		+0.00			+0.03		+0.10	

(Cp)(dHpe)(C≡C−C$_6$H$_5$) (**5-H**). Computational details are given in the Experimental Section.

Pertinent results on optimized geometries are shown in Table 5. Model **1-H** quite satisfactorily mimics the metric distances of the crystallographically characterized complex **1**, although the computed M−C and C−C distances are slightly shorter and longer, respectively, than the corresponding experimental values. The largest deviation concerns the Fe−P separations computed as 0.1 Å longer than that observed for **1**. These small deviations may be ascribed to some extent by the different substituents used for the computations, dHpe and C_5H_5 in **1-H** versus dppe and C_5Me_5 in **1**. The M−C and C−C distances computed for the mononuclear models **4** and **6-H** for which no X-ray data are available yet are very similar to those of model **1**. We simply note a slight contraction of the C−C separation on the alkynyl group bearing a hydrogen atom rather than an organometallic fragment, preventing any π-back-bonding to occur.

A comparison of the frontier MO energy level diagrams for the B3LYP-optimized complexes **1-H**, **4**, and **6-H** is given in Figure 3. In the mononuclear rhenium complex **4**, the LUMO 2a′ is heavily localized on the bpy ligand (95% in character), whereas most of the MOs in the HOMO region are delocalized on the rhenium−carbon backbone of the molecule. These MOs result from antibonding interactions between dπ orbitals of the rhenium fragment and in-plane ($\pi_{||}$) and out-of-plane ($\pi_{\perp}$) π orbitals of the 1,4-diethynylbenzene group. This is a common feature for carbon-group-containing organometallic species.[15,19]

In the iron species **6-H**, the LUMO 3a′ derives almost exclusively from π* components of the diethynylbenzene unit (91% in character). As for the rhenium complex, the HOMOs result from strong interactions between d-type metallic orbitals and π components of the carbon ligand. Importantly, in agreement with the more electron-releasing properties of the Fe group with respect to the Re entity, the HOMOs of **6-H** lie at substantially higher energy than the HOMOs of the rhenium species **4**.

The MO diagram of the rhenium−iron complex **1-H** is nearly the superimposition of the MO diagrams of the parent species. As for **4**, the LUMO 4a′ of **1-H** derives almost exclusively from π* components of the bpy ligand tethered to the Re center (95% bpy in character). As expected from the comparison of the energy of the HOMOs of the parent models **4** and **6-H**, the HOMOs in **1-H** are mainly iron and carbon ligand in character (see Figure 4). This leads to a

(18) Courmarcel, J.; Le Gland, G.; Toupet, L.; Paul, F.; Lapinte, C. *J. Organomet. Chem.* **2003**, *670*, 108.

(19) Weyland, T.; Lapinte, C.; Frapper, G.; Calhorda, M. J.; Halet, J. F.; Toupet, L. *Organometallics* **1997**, *16*, 2024.

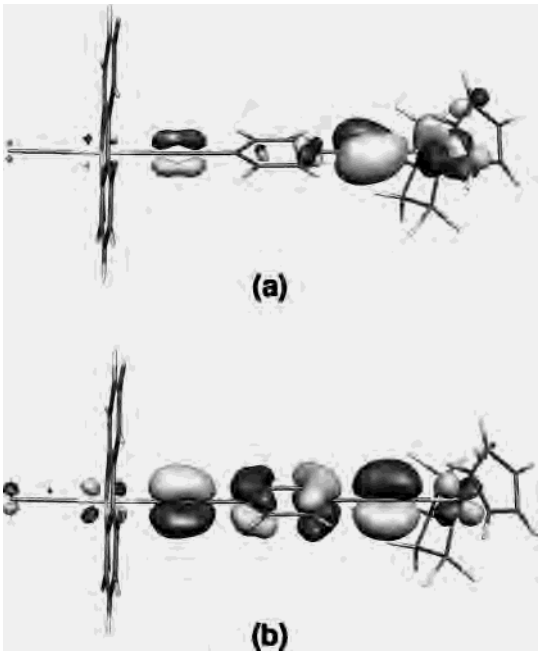

Figure 4. Contour plots of the HOMO (a) and HOMO − 1 (b) orbitals of **1-H** (contour value = 0.035 [e/bohr^3]$^{1/2}$).

smaller HOMO−LUMO gap in comparison to that computed for the rhenium parent model **4** without the terminal iron moiety (1.53 vs 2.17 eV for **1-H** and **4**, respectively). The MOs deriving from the rhenium part are found to be low in energy. Importantly, the weak contribution of rhenium in the HOMOs deriving from the iron group and, vice versa, the very poor participation of iron in the MOs below the HOMOs, which mainly descend from the rhenium entity, indicate a quite moderate electronic communication between the two metallic centers in **1-H**.

This moderate electronic communication between the metal centers is also illustrated by the comparison of Mulliken atomic net charges of the metal atoms for the different complexes (see Table 5). The values for rhenium and iron are nearly identical in **1-H** and in their respective parent complexes (ca. 0.70 for Re and −0.60 for Fe). The more sterically hindered carbon atoms in the α position of the metal centers are less negatively charged than those in β position (−0.10 (Re) and 0.05 (Fe) vs −0.37 (Re) and −0.27 (Fe)). The nucleophilic nature of the β carbon atoms with respect to the α ones is in close agreement with the addition of the proton at the former in complex **3**.

M−C and C−C separations were compared for different molecular charges of **1-H** (see Table 5). Owing to the nodal properties of the LUMO of **1-H** (see preceding discussion), one-electron reduction of **1-H** hardly changes atomic distances of the metal−carbon backbone. As shown in Table 5, the unpaired electron of [**1-H**]$^-$ is nearly exclusively localized on the bipyridine ligand. On the other hand, some structural changes are observed upon oxidation of **1-H** to [**1-H**]$^+$ with some lengthening of the C≡C bonds and some strengthening of the Fe−C bond. Surprisingly enough, these geometrical changes, expected from the nodal properties of the HOMO and HOMO − 1, are not reproduced in the corresponding experimental cationic compound **2**. Rather high esd's on the distances measured experimentally for **1** and **2** prevent any conclusions concerning this point.

The unpaired electron of [**1-H**]$^+$ is delocalized over the iron and the carbon linker with more than half of the spin density found on the iron center, and the rest on the carbon chain (see Table 5). Nevertheless, the SOMO of [**1-H**]$^+$ is mainly localized on the carbon spacer and on the rhenium atom (21%). The admixture of iron is very weak (2%) in constrast to the HOMOs of the neutral complex **1-H**. This spin-orbital derives in turn mainly from the HOMO − 3 of **1-H** which features an appreciable component from Re. On the other hand, the lowest unoccupied spin-orbital derives mainly from the HOMO − 1 of **1-H** and contains a rather high Fe character (35%). The participation of Re is weak (3%), confirming that the oxidation of **1-H** affects the iron center and the carbon chain. The next unoccupied spin-orbitals are localized on the bpy ligand, analogously to the LUMO of the neutral parent molecule. The significant change in the electronic structure observed for [**1-H**]$^+$ with respect to that of **1-H** must play an important role in the nature of the luminescence properties discussed later.

The first adiabatic ionization potential (IP) of **1-H**, **5-H**, and **6-H** was computed as the difference between the total energies of the radical cation and the corresponding neutral minima (see Table 5). Comparison of the data indicates that the heterobimetallic species **1-H** is more readily ionized than its mononuclear iron counterparts, **5-H** and **6-H** (e.g., 5.19 vs 5.58 and 5.92 eV). As mentioned earlier, this reflects the electron-releasing nature of the rhenium endgroup toward the opposite iron endgroup, facilitating the oxidation. The first adiabatic electron affinity (EA) of **1-H**, obtained from the difference between the total energies of the neutral and the corresponding radical anion minima, was also calculated and compared to that of the parent model complex **4** (see Table 5). Iron endgroup attachment in **1-H** contributes to a slight decrease in the electron affinity with respect to that of the mononuclear Re complex **4** (e.g., 1.67 vs 1.85 eV). This shows that this iron endgroup acts as an electron-releasing group toward the opposite endgroup making the reduction slightly more difficult. These results fully support the cyclic voltammetry data which show the same trend (see preceding discussion).

UV−Visible and NIR Absorption Spectroscopy. The electronic absorption spectrum of the heterobimetallic complex **1** shows a high-energy absorption band at 290 nm and a low-energy band at 390 nm with a 420-nm shoulder in dichloromethane solution at room temperature (Table 6 and Figure 5). The high-energy band is assigned to intraligand (IL) $\pi \rightarrow \pi^*$ transitions of 1,4-diethynylbenzene and bipyridine ligands since the free ligands also absorb strongly at similar energies. With reference to the electronic absorption studies of the related precursors, [(C_5Me_5)(dppe)Fe(C≡C−C_6H_5)][12] and [Re(CO)$_3$(bpy)(C≡C−C_6H_4−C≡CH)],[10] which show low-energy absorptions at 348 and 420 nm, respectively, the low-energy absorptions of **1** are tentatively assigned as an admixture of dπ(Fe) → π^*(C≡C), dπ(Re) → π^*(C≡C), and dπ(Re) → π^*(bpy) metal-to-ligand charge transfer (MLCT) transitions. This is in agreement with the

Table 6. UV−Vis and NIR Absorption and Emission Spectral Data of Complexes **1**−**3** and Their Related Precursor Complexes in CH_2Cl_2 at 298 K

complex	absorption λ_{abs}/nm (ϵ/dm^{3}mol^{-1}cm^{-1})	emission λ_{em}/nm
1	290 (39 900), 390 (22 000), 420 sh (20 100)	nonemissive
2	292 (49 000), 340 sh (25 300), 432 (9 100), 474 sh (7 500), 830 (7 600), 1389 (22), 1773 (210)	590
3	300 (41 100), 348 (43 600), 358 (46 000), 420 (3 805)	605
4	298 (49 740), 328 sh (28 640), 420 (2 860)	650
5	245 (34 000), 348 (12 000)	not measured
5$^+$	241 (34 000), 267 (37 000), 575 (2 200), 663 (2 900)	not measured

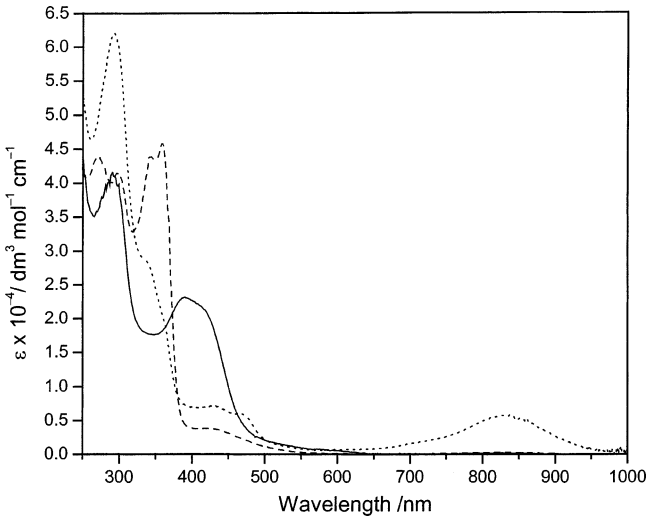

Figure 5. UV−vis spectra of **1** (—), **2** (···), and **3** (- - -) in dichloromethane solution at room temperature.

atomic character of the HOMOs and LUMOs of **1-H** (see preceding description).

Upon one-electron oxidation at the iron center, complex **1** was converted to radical cation **2**, and the intense band at ca. 390−420 nm in **1** was replaced by two less intense bands at ca. 432 and 474 nm. It is likely that, upon one-electron oxidation of Fe^{II} to Fe^{III}, the band due to the dπ(Fe) → π*(C≡C) MLCT transition would vanish, leaving behind the dπ(Re) → π*(bpy) and dπ(Re) → π*(C≡C) MLCT transitions. Similar loss of the dπ(Fe) → π*(C≡C) MLCT intensities has been reported in the oxidation of the related compound, [(C_5Me_5)(dppe)Fe(C≡C−C_6H_5)] to [(C_5Me_5)(dppe)Fe(C≡C−C_6H_5)](PF_6).[15] The resolution of two bands at ca. 432 and 474 nm in **2** may be a result of the slight red shift of the dπ(Re) → π*(C≡C) MLCT band upon oxidation of the electron-rich Fe^{II} center to Fe^{III}, which may be viewed as an electron-deficient substituent on the 1,4-diethynylbenzene unit. In addition, the radical cation **2** exhibits a low-energy absorption at ca. 830 nm with a shoulder at ca. 726 nm. These low-energy absorption bands are ascribed to the ligand-to-metal charge transfer (LMCT) transition derived from the [(C_5Me_5)(dppe)Fe^{III}(C≡C−C_6H_4−C≡C)]− moiety. Similar LMCT absorption bands have also been observed in the related complexes, [(C_5Me_5)(dppe)Fe(C≡C−C_6H_4−C≡C)Fe(C_5Me_5)(dppe)](PF_6) at 546 and 702 nm,[18] [(C_5Me_5)(dppe)Fe(C≡C−C≡C)Fe(C_5Me_5)(dppe)](PF_6) at 619 and 845 nm,[20] and a heterobimetallic rhenium−iron complex, (C_5Me_5)Re(NO)(PPh_3)(C≡C−C≡C)Fe(C_5Me_5)(dppe)](PF_6) at 868 nm.[8]

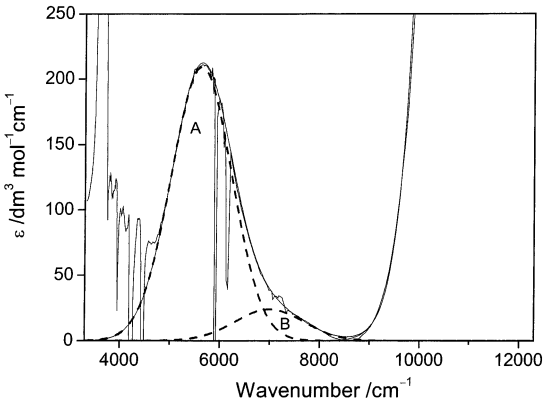

Figure 6. NIR spectrum of **2** (—) in dichloromethane at 20 °C, with deconvoluted bands (- - -).

The UV−vis spectrum of the iron−vinylidene complex **3** in dichloromethane shows only one low-energy absorption band at ca. 420 nm. In view of the close resemblance of the band shape, band energy, and extinction coefficient with its precursor complex, [$Re(CO)_3$(bpy)(C≡C−C_6H_4−C≡CH)], the low-energy absorption band at 420 nm is assigned as a dπ(Re) → π*(bpy) MLCT transition.

The radical cation **2** also exhibits a weak NIR absorption band at 1773 nm with a shoulder at 1389 nm. Assuming that the absorption bands have Gaussian profiles, the spectrum of **2** was deconvoluted in the range 3500−10000 cm^{-1}. As shown in Figure 6, results show good agreement between the experimental spectrum and the sum of the spectral components. The band shape analysis reveals the presence of two absorption bands in addition to the tail of the MLCT bands. The more intense band centered at 5665 cm^{-1} (1773 nm, ϵ = 210 dm^3 mol^{-1} cm^{-1}, $\Delta\nu_{1/2}$= 1710 cm^{-1}) is similar to that invariably observed in the NIR spectra of mononuclear Fe^{III} species.[21] For instance, the NIR spectrum of complex **5**$^+$ displays a band at 1830 nm (ϵ = 90 dm^3 mol^{-1} cm^{-1}, $\Delta\nu_{1/2}$ = 1830 cm^{-1}). Such a band was assigned to a ligand field forbidden transition; therefore, it is unlikely that the band at 5665 cm^{-1} corresponds to IVCT transition. The second component of the spectrum located at higher energy (7000 cm^{-1} (1389 nm), ϵ = 22 dm^3 mol^{-1} cm^{-1}, $\Delta\nu_{1/2}$= 1940 cm^{-1}) was never observed in any monometallic Fe^{III} derivatives. Considering that this NIR absorption band is characteristic of an IVCT band for a weakly coupled system, it can be assigned to an Fe^{III}−Re^{I} metal-to-metal charge transfer transition. In the case of nonsymmetric mixed-valence system **2**, the redox centers are weakly coupled as shown from IR, Mössbauer, and ESR spectroscopies, and the Hush model applies.[22,23] The electronic coupling parameter V_{ab} can then be computed in cm^{-1}

(20) Le Narvor, N.; Toupet, L.; Lapinte, C. *J. Am. Chem. Soc.* **1995**, *117*, 7129.
(21) Weyland, T.; Costuas, K.; Toupet, L.; Halet, J. F.; Lapinte, C. *Organometallics* **2000**, *19*, 4228.
(22) Hush, N. S. *Trans. Faraday Soc.* **1961**, *57*, 557.
(23) Hush, N. S. *Prog. Inorg. Chem.* **1967**, *8*, 391.

using eq 1, where R_{FeRe} is the through space metal−metal distance (Å). This formula yields 30 cm^{-1} for the electronic coupling.

$$V_{ab} = 0.0205(\epsilon_{max}\nu_{max}\Delta\nu_{1/2})^{1/2}/R_{MM'} \quad (1)$$

$$(\Delta\nu_{1/2})_{theo} = [2300(\nu_{max} - \Delta G_0)]^{1/2} \quad (2)$$

$$\lambda = E_{op} - \Delta G_0 \quad (3)$$

$$\Delta G^{\ddagger} = (\lambda - 2V_{ab})^2/4\lambda \quad (4)$$

As the electronic coupling in this system is small, it can be assumed that the bandwidth computed from the Hush theory should be very close to the experimental value. Equation 2 can then be used to calculate the free energy difference (ΔG_0) between the ground state [Fe^{III}]−L−[Re^{I}] and the excited state [Fe^{II}]−L−[Re^{II}]. The value obtained (5370 cm^{-1}) is large with respect to the vertical energy of reorganization (λ = 1630 cm^{-1}) which represents the Frank−Condon barrier. As the value of λ is smaller than ΔG_0, the activation energy cannot be computed.[24]

Luminescence Spectroscopy. Unlike the related rhenium(I)−alkynyl complex, [$Re(CO)_3$(bpy)(C≡C−C_6H_4−C≡CH)], which exhibits rich luminescence properties derived from the [dπ(Re) → π*(bpy)] ^{3}MLCT excited state upon photoexcitation, the heterobimetallic rhenium(I)−iron(II) complex **1** is nonemissive both in the solid state and in fluid solution. The lack of emission property in **1** may be attributed to intramolecular quenching processes. A likely process is reductive electron transfer quenching. Assuming the heterobimetallic complex has behavior similar to the individual precursor complexes, [$Re(CO)_3$(bpy)(C≡C−C_6H_4−C≡CH)] and [(C_5Me_5)(dppe)Fe(C≡C−C_6H_4−C≡CH)], an estimation of the excited-state reduction potential using spectroscopic $E_{0-0}(Re^{*/0})$ of 2.37 eV and electrochemical data $E°(Re^{0/-})$ of −1.47 V versus SCE of [$Re(CO)_3$(bpy)(C≡C−C_6H_4−C≡CH)] would predict a ^{3}MLCT excited-state reduction potential $E°(Re^{*/-})$ of +0.9 V versus SCE. With a $E°(Fe^{III/II})$ of −0.11 V versus SCE for [(C_5Me_5)(dppe)Fe(C≡C−C_6H_4−C≡CH)],[18] a huge driving force of >+1.0 V is estimated for the reductive electron transfer quenching process. Attempts to probe the intermolecular quenching reaction between [$Re(CO)_3$(bpy)(C≡C−C_6H_4−C≡CH)] and [(C_5Me_5)(dppe)Fe(C≡C−C_6H_4−C≡CH)] were unsuccessful since the quencher, [(C_5Me_5)(dppe)Fe(C≡C−C_6H_4−C≡CH)], absorbs both at the excitation and emission wavelength of [$Re(CO)_3$(bpy)(C≡C−C_6H_4−C≡CH)], rendering corrections for light excitation and emission due to self-absorption effects difficult. Attempts to determine the bimolecular quenching rate constant using time-resolved emission studies were also not possible since the measurement of the relatively short emission lifetime (in the nanosecond range) of the system was limited by our instrument. However, on the basis of an estimation of the driving force, it is very likely that intramolecular reductive electron transfer quenching did occur, rendering complex **1** nonemissive. As already mentioned, DFT calculations on **1-H** also reveal that the Fe(II) center, being electron-rich, has a higher-lying dπ orbital than that of the Re(I) center (see Figure 3), which has further been supported by cyclic voltammetric data. Thus, the presence of low-lying MLCT and LF excited states of the iron moiety would readily quench the ^{3}MLCT emission of the rhenium bipyridyl core, either by nonradiative interstate crossing, energy transfer, or electron transfer processes.

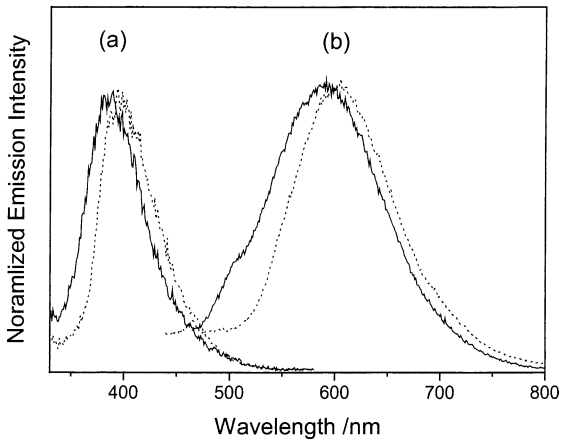

Figure 7. The excitation (a) and emission (b) spectra of **2** (—) and **3** (···) in dichloromethane at room temperature.

The one-electron oxidized radical cation **2** and the vinylidene analogue **3** both emit in dichloromethane solution with emission maxima at 590 and 605 nm, respectively. Figure 7 displays the emission and excitation spectra of **2** and **3** in dichloromethane at room temperature. On the basis of the observation that the excitation peak maximum occurs at ca. 400 nm and our previous spectroscopic studies on the rhenium(I)−alkynyl system,[6,10] an assignment of the emission as derived from the dπ(Re) → π*(bpy) ^{3}MLCT excited state was made. The recovery of emission behavior in both complexes **2** and **3** can be ascribed to the fact that both the Fe^{III} and the iron vinylidene are electron-deficient and are not good electron donors and, thus, no reductive electron-transfer quenching can occur. This can also be reflected by the blue shift of the ^{3}MLCT emission bands in **2** and **3** relative to the related mononuclear complex, [$Re(CO)_3$(bpy)(C≡C−C_6H_4−C≡CH)] (**4**) which exhibits an emission band at ca. 650 nm. Since both the iron(III) metal center and the iron vinylidene unit in **2** and **3**, respectively, with an overall positive charge of +1 can be regarded as electron-withdrawing substituents on the 1,4-diethynylbenzene unit, the alkynyl group would behave as a poorer σ as well as π donor, lowering the energy level of the dπ(Re) orbital, and resulting in a shift of the ^{3}MLCT energy to higher energy. Such a blue shift in emission energy is consistent with the assignment of a ^{3}MLCT emission origin. Similarly, one can visualize this as the stabilization of the dπ(Fe) orbital in the Fe^{III} state in **2** as well as in the relatively electron-deficient iron vinylidene in **3**, which would lead to the absence of low-lying LF and MLCT states that would quench the emission. Thus, it is envisaged that the present system could be considered as a redox "switch" capable of switching on and off the triplet photoluminescence of this heterobimetallic complex system.

(24) Brunschwig, B. S.; Sutin, N. *Coord. Chem. Rev.* **1999**, *187*, 233.

Experimental Section

Materials and Reagents. All manipulations were carried out under an inert atmosphere of argon. KPF_6 (99.5%) and ^{t}BuOK (95%) were obtained from Strem and Aldrich Chemical Co., respectively. $[Re(CO)_3(bpy)(C{\equiv}C{-}C_6H_4{-}C{\equiv}C{-}H)]$ (**4**),[10] $[Fe(C_5Me_5)(dppe)Cl]$ (**7**),[9] and $[Cp_2Fe][PF_6]$[25] were prepared according to literature procedures. All solvents were purified and distilled using standard procedures before use. All other reagents were of analytical grade and were used as received. High field NMR experiments were performed on a multinuclear Bruker 400, 300, or 200 MHz instrument (DPX400, AM300WB, and 200DPX). Chemical shifts are given in parts per million relative to tetramethylsilane (Me_4Si) for ^{1}H and ^{13}C NMR spectra, and 85% H_3PO_4 for ^{31}P NMR spectra. Transmittance-FTIR spectra were recorded using a Bruker IFS28 spectrometer or a Bio-Rad FTS-7 spectrometer (400−4000 cm^{-1}). UV−vis spectra were recorded on an UVIKON 942 or Hewlett-Packard HP8452 spectrophotometer. Steady-state excitation and emission spectra were obtained on a Spex Fluorolog 111 spectrofluorometer. Cyclic voltammograms were recorded using a PAR 263 in CH_2Cl_2 (0.1 M (^{n}Bu)$_4$N$^+$PF$_6^-$) at 25 °C at a platinum electrode, using an SCE reference electrode and ferrocene as internal calibrant (0.460 V).[25] Mössbauer spectra were recorded with a 2.5×10^{-2} C (9.25×10^8 Bq) ^{57}Co source using a symmetric triangular sweep mode.[26,27] LSI-MS analyses were effected at the "Centre Regional de Mesures Physiques de l'Ouest" (Rennes; CRMPO) on a high-resolution MS/MS ZabSpec TOF Micromass spectrometer (8 kV). Elemental analyses were performed at the Centre for Microanalyses of the CNRS at Lyon-Solaise, France, or on a Carlo Erba 1106 elemental analyzer at the Institute of Chemistry of the Chinese Academy of Sciences in Beijing.

$[Re(CO)_3(bpy)(C{\equiv}C{-}C_6H_4{-}C{\equiv}C)Fe(C_5Me_5)(dppe)]$ (1). A mixture of $[Re(CO)_3(bpy)(C{\equiv}C{-}C_6H_4{-}C{\equiv}C{-}H)]$ (**4**) (0.200 g, 0.36 mmol), $[Fe(C_5Me_5)(dppe)Cl]$ (**7**) (0.250 g, 0.40 mmol), KPF_6 (0.080 g, 0.43 mmol), and ^{t}BuOK (0.049 g, 0.44 mmol) in THF−MeOH (40 mL, 1:3 v/v) was stirred at room temperature for 2 days. The reaction mixture was evacuated to remove the solvent, and the residue was extracted with toluene (20 mL). Subsequent removal of the solvent followed by washing with MeOH afforded a brownish yellow solid, which was recrystallized from CH_2Cl_2−MeOH to give brown crystals of **1** (0.165 g, 40% yield). ^{1}H NMR (δ, 400 MHz, CD_2Cl_2, 298 K): 1.38 (s, 15 H, C_5Me_5), 1.92 (m, 2 H, PCH_2), 2.55 (m, 2 H, PCH_2), 6.30 (d, 2 H, $-C_6H_4-$), 6.72 (d, 2 H, $-C_6H_4-$), 7.38 (m, 16 H, PPh_2), 7.60 (t, 2 H, $J = 6.6$ Hz, 4- and 4′-bipyridyl Hs), 7.85 (m, 4 H, PPh_2), 8.15 (t, 2 H, $J = 7.8$ Hz, 5- and 5′-bipyridyl Hs), 8.30 (d, 2 H, $J = 8.0$ Hz, 3- and 3′-bipyridyl Hs), 9.15 (d, 2 H, $J = 5.5$ Hz, 6- and 6′-bipyridyl Hs). Anal. Calcd for $C_{59}H_{51}FeN_2O_3P_2Re{\cdot}MeOH$: C, 61.48; H, 4.73; N, 2.39. Found: C, 61.39; H, 4.51; N, 2.24. MS (positive LSI, 3-NBA) 1140 (**1**$^+$, 96%), 714 ($[(C_5Me_5)(dppe)FeCC{-}C_6H_4{-}CC]^+$, 77.5%), 589 ($[(C_5Me_5)(dppe)Fe]^+$, 100%).

$[Re(CO)_3(bpy)(C{\equiv}C{-}C_6H_4{-}C{\equiv}C)Fe(C_5Me_5)(dppe)]^+[PF_6]^-$ (2). A Schlenk flask was charged with (**1**) (0.200 g, 0.18 mmol), $[Cp_2Fe]^+[PF_6]^-$ (0.055 g, 0.17 mmol), and THF (30 mL). The mixture was stirred at −80 °C for 6 h. *n*-Hexane (30 mL) was added to precipitate the green product, which was then filtered, and the residue was washed with diethyl ether (3 × 20 mL). Complex **2** was obtained as a spectroscopically pure green powder in 82% (0.202 g) yield. Subsequent recrystallization from dichloromethane−*n*-hexane gave green crystals of **2** (0.083 g, 37%). Anal. Calcd for $C_{59}H_{51}F_6FeN_2O_3P_3Re{\cdot}5/4CH_2Cl_2$: C, 52.02; H, 3.88; N, 2.01. Found: C, 52.22; H, 3.74; N, 1.86.

$[Re(CO)_3(bpy)(C{\equiv}C{-}C_6H_4{-}(H)C{=}C{=})Fe(C_5Me_5)(dppe)]^+[PF_6]^-$ (3). A Schlenk tube was charged with (**4**) (0.152 g, 0.276 mmol), 1.2 equiv of (**7**) (0.207 g, 0.331 mmol), 1.2 equiv of KPF_6 (0.061 g, 0.331 mmol), and 20 mL of THF. After dissolution of the solids, 60 mL of methanol was added. The mixture was stirred for 24 h at 20 °C. The solvents were then cryogenically trapped, and the solid residue was extracted with dichloromethane. After concentration to 10 mL, 100 mL of *n*-pentane was added to precipitate a brown powder. Washings with 3 × 20 mL of *n*-pentane yielded complex **3** in pure form (0.206 g, 75%). ^{1}H NMR (δ, 200 MHz, $CDCl_3$, 298 K): 9.05 (d, 2 H, $^3J_{HH} = 5.1$ Hz, 6- and 6′-bipyridyl Hs); 8.49 (d, 2 H, $^3J_{HH} = 7.9$ Hz, 3- and 3′-bipyridyl Hs); 8,1 (t, 2 H, $^3J_{HH} = 7.6$ Hz, 5- and 5′-bipyridyl Hs); 7.56 (d, 2 H, $^3J_{HH} = 6.5$ Hz, 4- and 4′-bipyridyl Hs); 7.5−7.00 (m, 20H, PPh_2); 6.47 (d, 2 H, $^3J_{HH} = 8.1$ Hz, $-C_6H_4-$); 5.96 (d, 2 H,$^3J_{HH} = 7.9$ Hz, $-C_6H_4-$); 4.98 (t, 1 H,$^4J_{PH} = 3.5$ Hz, HC═C−); 3.01−2.37 (2m, 4 H, PCH_2); 1.52 (s, 15 H, C_5Me_5). ^{13}C NMR (δ, 75 MHz, CD_3COCD_3, 298 K, Me_4Si ext): 363 (t, $^2J_{CP} = 34$ Hz, Fe═C═); 206.1 (s, CO); 199.8 (s, CO); 193.9 (s, CO); 156.8 (m, C_5H_4N); 153.9 (ddd, $^1J_{CH} = 189$ Hz, $^2J_{CH} = 5$ Hz, C_5H_4N); 140 (dd, $^1J_{CH} = 169$ Hz, $^2J_{CH} = 6$ Hz, C_5H_4N); 134.6−128.1 (m, Ph); 127.4 (dd, $^1J_{CH} = 160$ Hz, C_5H_4N); 126.5 (m,$^1J_{CH} = 156$ Hz, Fe═C═*C*); 124.7 (s, Re−C≡); 106 (s, Re−C≡*C*); 101 (s, C_5Me_5); 30 (m, PCH_2); 10.5 (q, $^1J_{CH} = 128$ Hz, C_5Me_5). ^{31}P{^{1}H} NMR (δ, 81 MHz, $CDCl_3$, 298 K): 88.8 (s, dppe). MS (positive LSI, *o*-NPOE) 1141, 1140 (**3**$^+$, **3**$^+$ − H, 4%), 589 ($[(C_5Me_5)(dppe)Fe]^+$, 100%).

X-ray Crystallography. Single crystals of **1** and **2** were obtained by slow diffusion of methanol and *n*-hexane into dichloromethane solutions of **1** and **2**, respectively. A crystal of dimensions 0.4 × 0.25 × 0.1 mm^3 (0.5 × 0.3 × 0.2 mm^3 for **2**) mounted in a glass capillary was used for data collection at 28 °C on a MAR diffractometer with a 300 mm image plate detector using graphite monochromatized Mo Kα radiation ($\lambda = 0.71073$ Å). Data collection was made with 2° oscillation step of φ, 300 s (420 s for **2**) exposure time, and scanner distance at 120 mm to have totally 100 images collected. The images were interpreted and intensities integrated using the program DENZO.[28] For **1**, the structure was solved by direct methods employing the SHELXS-97 program[29] on a PC. All atoms were located according to the direct methods. The positions of the other non-hydrogen atoms were found after successful refinement by full-matrix least-squares using the program SHELXL-97[30] on a PC. All 9907 independent reflections from a total 21402 reflections participated in the full-matrix least-squares refinement against F^2. These reflections were in the range of $2\theta_{max}$ equal to 51.16° (*h*, −13 to 13; *k*, −18 to 18; *l*, −20 to 21). One crystallographic asymmetric unit consists of one formula unit including two CH_2Cl_2 solvent molecules. In the final stage of least-squares refinement, the non-hydrogen atoms of dichloromethane solvent molecules were refined isotropically, other non-hydrogen atoms anisotropically. Hydrogen atoms except those of the CH_2-

(25) Connelly, N. G.; Geiger, W. E.; *Chem. Rev.* **1996**, *96*, 877.
(26) Varret, F.; Mariot, J. P.; Hamon, J. R.; Astruc, D. *Hyperfine Interact.* **1988**, *39*, 67.
(27) Greenwood, N. N. *Mössbauer Spectroscopy*; Chapman and Hall: London, 1971.
(28) Written with the cooperation of the program authors Otwinowski, Z., and Minor, W.: Gewirth, D. *DENZO: "The HKL Manual−A description of programs DENZO, XDISPLAYF, and SCALEPACK"*; Yale University: New Haven, 1995 .
(29) SHELXS97: Sheldrick, G. M. *SHELXS97: Programs for Crystal Structure Analysis (release 97-2)*; University of Göttingen: Göttingen, Germany, 1997.
(30) SHELXL97: Sheldrick, G. M. *SHELXL97: Programs for Crystal Structure Analysis (release 97-2)*; University of Göttingen: Göttingen, Germany, 1997.

Cl_2 solvent molecules were generated by program SHELXL-97.[30] The positions of H atoms are calculated on the basis of the riding mode with thermal parameters equal to 1.2 times that of the associated C atoms, and participated in the calculation of final *R*-indices. For **2**, the structure was solved by direct methods employing the SIR-97 program[31] on a PC. Most non-hydrogen atoms were located according to the direct methods and the successive least-squares Fourier cycles. The positions of the other non-hydrogen atoms were found by successful full-matrix least-squares refinements and successive difference Fourier synthesis using program SHELXL-97[30] on a PC. All 10063 independent reflections from a total 29932 reflections participated in the full-matrix least-squares refinement against F^2. These reflections were in the range of $2\theta_{max}$ equal to 51.20° (*h*, −15 to 14; *k*, −17 to 18; *l*, −40 to 40). One crystallographic asymmetric unit consists of one formula unit, including one anion, and one and a half CH_2Cl_2 solvent molecules. In the final stage of least-squares refinement, all non-hydrogen atoms were refined anisotropically. Hydrogen atoms were generated by the program SHELXL-97. The positions of hydrogen atoms were calculated on the basis of the riding mode with thermal parameters equal to 1.2 times that of the associated C atoms, and participated in the calculation of final *R*-indices.

Theoretical Calculations. Calculations were carried out at the B3LYP level of density functional theory as implemented in the Gaussian-98 suite of programs.[17] The model complexes of C_s symmetry, Re(bpy)$(CO)_3$(C≡C−C_6H_4−C≡C)Fe(Cp)(dHpe) (**1-H**), Re(bpy)$(CO)_3$(C≡C−C_6H_4−C≡CH) (**4**), and Fe(Cp)(dHpe)(C≡C−C_6H_4−C≡CH) (**6-H**), were fully optimized with the LANL2DZ basis set and an additional set of polarization functions as introduced by Hay and Wadt.[32]

Acknowledgment. We acknowledge the award of a grant by the CNRS/RGC under the PROCORE: France-Hong Kong Joint Research Scheme. V.W.-W.Y. acknowledges financial support from The University of Hong Kong Foundation for Educational Development and Research Limited, the Research Grants Council of the Hong Kong Special Administrative Region, China (Project HKU 7123/00P), and the receipt of a Croucher Senior Research Fellowship from the Croucher Foundation. S.C.-F.L. acknowledges the receipt of a postgraduate studentship from The University of Hong Kong and a Li Po Chun Postgraduate Scholarship from the Li Po Chun Charitable Fund, and C.-C.K. acknowledges the receipt of a Croucher Scholarship from the Croucher Foundation and a Li Po Chun Postgraduate Scholarship from the Li Po Chun Charitable Fund. K.M.-C.W. and N.Z. acknowledge the receipt of University Postdoctoral Fellowships, which are administered by The University of Hong Kong. The ATCO company is acknowledged for financial support to S.R., J.-F.H., K.C., S.K., and S.F. acknowledges the Center de Resources Informatiques (CRI, Rennes) for computing facilities. S.F. thanks Pr. A. Boucekkine (Rennes) for computational assistance.

Supporting Information Available: Crystallographic data for **1** and **2**. This material is available free of charge via the Internet at http://pubs.acs.org.

IC030226D

(31) Altomare, A.; Burla, M. C.; Camalli, M.; Cascarano, G.; Giacovazzo, C.; Guagliardi, A.; Moliterni, A. G. G.; Polidori, G.; Spagna, R. Sir97: a new tool for crystal structure determination and refinement. *J. Appl. Crystallogr.* **1998**, *32*, 115−119.

(32) (a) Hay, P. J.; Wadt, W. R. *J. Chem. Phys.* **1985**, *82*, 299. (b) Dunning, T. H., Jr.; Hay, P. J. In *Modern Theoretical Chemistry*; Schaefer, H. F., III, Ed.; Plenum: New York, 1976, 1. For polarization functions see: Huzinaga, S.; Anzelm, J.; Klobukowski, M.; Radzio-Andzelm, E.; Sakai, Y.; Tatewaki, H. *Gaussian Basis Sets for Molecular Calculations*; Elsevier: Amsterdam, 1984.